Available online at www.sciencedirect.com

SCIENCE DIRECT®

Lithos 77 (2004) 593–608

LITHOS

www.elsevier.com/locate/lithos

Layered mantle at the Karelian Craton margin: *P–T* of mantle xenocrysts and xenoliths from the Kaavi–Kuopio kimberlites, Finland

M.L. Lehtonen*, H.E. O'Brien, P. Peltonen, B.S. Johanson, L.K. Pakkanen

Geological Survey of Finland, P.O. Box 96, FIN-02151 Espoo, Finland

Received 27 June 2003; accepted 5 November 2003
Available online 18 May 2004

Abstract

Peridotitic clinopyroxene (cpx) and pyrope garnet xenocrysts from four kimberlite pipes in the Kaavi–Kuopio area of Eastern Finland have been studied using major and trace element geochemistry to obtain information on the vertical compositional variability of the underlying mantle. The xenocryst data, when combined with the petrological constraints provided by peridotite xenoliths, yield a relatively complete section through the lithospheric mantle. Single-grain cpx thermobarometry fits with a 36-mW/m^2 geotherm calculated using heat flow constraints and xenolith modes and geophysical properties. Ni thermometry on pyrope xenocrysts gives 700–1350 °C and, based on the cpx xenocryst/xenolith geotherm, indicates a wide sampling interval, ca. 80–230 km. Plotting pyrope major and trace element compositions as a function of temperature shows there are three distinct layers in the local lithospheric mantle:

(1) A low-temperature (<850 °C) harzburgite layer distinguished by Ca-rich but Ti-, Y- and Zr-depleted pyropes. The xenoliths originating from this layer are all fine-grained garnet-spinel harzburgites with secondary cpx.
(2) A variably depleted lherzolitic, harzburgitic and wehrlitic horizon from 950 to 1150 °C or 130 to 180 km.
(3) A deep layer from 180 to 240 km composed largely of fertile material.

The peridotitic diamond window at Kaavi–Kuopio stretches from the top of the diamond stability field at 140 km to the base of the harzburgite-bearing mantle at about 180 km, implying a roughly 40-km-wide prospective zone.

Keywords: Kimberlite; Xenocryst; Xenolith; Lithosphere; Thermobarometry; Karelian Craton

1. Introduction

The Kaavi–Kuopio Kimberlite Province situated at the edge of the Karelian Craton comprises two distinct kimberlite clusters containing at least 19 kimberlites with mineralogy typical of Group I kimberlite (Tyni, 1997; O'Brien and Tyni, 1999). The pipes have intruded Archean (3.5–2.6 Ga) basement gneisses and allochthonous Proterozoic (1.9–1.8 Ga) metasediments (Kontinen et al., 1992; Fig. 1). Several methods have been used to date the

* Corresponding author. Fax: +358-20-550-12.
E-mail address: marja.lehtonen@gsf.fi (M.L. Lehtonen).

0024-4937/$ - see front matter © 2004 Elsevier B.V. All rights reserved.
doi:10.1016/j.lithos.2004.04.026

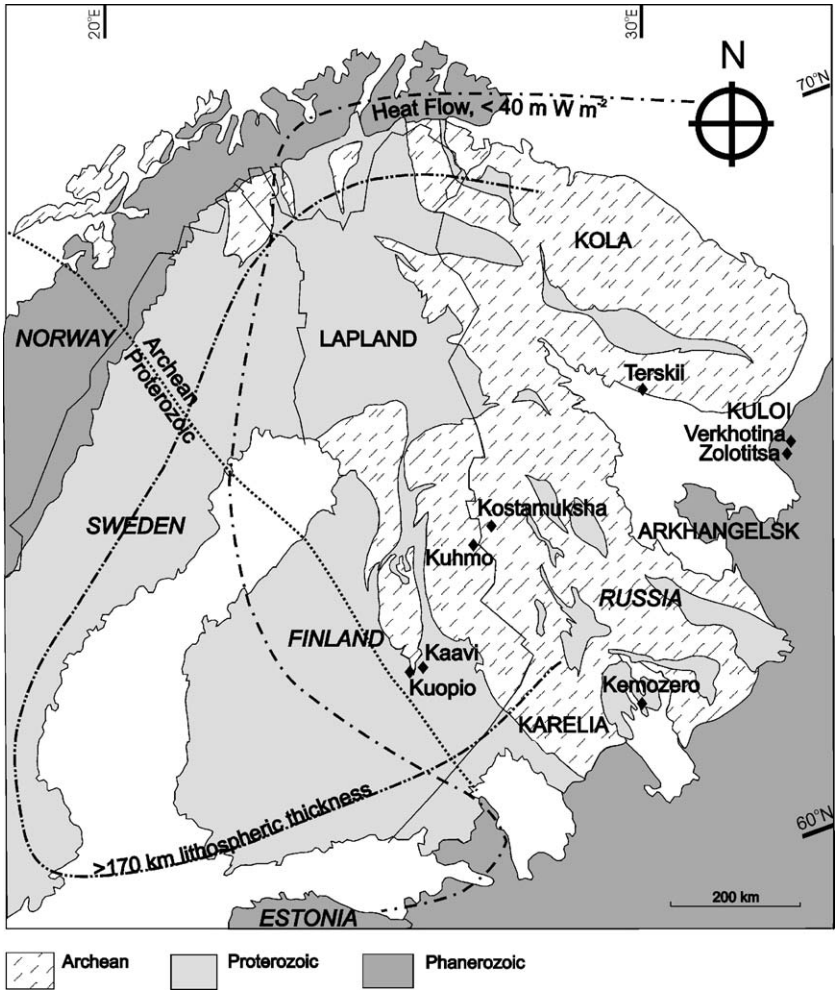

Fig. 1. Map illustrating the diamond prospective area of Northern Europe characterized by (a) low heat flow (simplified from Kukkonen and Jõeleht, 1996) and (b) lithosphere thicker than 170 km based on seismic data (Calcagnile, 1982). Generalized geology modified after Gaál and Gorbatschev (1987). The Archean/Proterozoic boundary marks the subsurface extent of the Archean craton. The black diamonds represent diamond-bearing kimberlites and lamproites.

kimberlite magmatism (Tyni, 1997; Peltonen et al., 1999; Peltonen and Mänttäri, 2001), but the U–Pb ion probe ages of 589–626 Ma from perovskites (O'Brien et al., in press) are considered to be the most reliable. Mantle xenoliths from the Kaavi–Kuopio pipes have been studied by Peltonen et al. (1999), and a geotherm of 36 mW/m^2 has been calculated using heat flow constraints and xenolith modes and geophysical properties (Kukkonen and Peltonen, 1999). The xenolith suite provides evidence of a compositionally stratified lithospheric mantle adjacent to the ancient suture zone between the Archean Karelian Craton and the Proterozoic Svecofennian mobile belt. A shallow zone (<900 °C) of garnet-spinel harzburgites is underlain by a zone of garnet facies peridotites (180–240 km) including lherzolitic, harzburgitic, olivine websteritic and wehrlitic varieties (Peltonen et al., 1999). Mantle eclogite xenoliths are also present, some of them being highly diamondiferous (Peltonen et al., 2002). The upper mantle beneath the Karelian Craton is interpreted to have a mixed origin, consisting of remnants of thinned Archean subcontinental lithospheric mantle, possibly underlain by early Protero-

zoic lithosphere and/or younger material underplated around 1.8 Ga (Peltonen et al., 1999). The small number of xenoliths available gives a limited sampling of the lithosphere relative to the xenocryst record. The aim of this study was therefore to obtain additional information on the vertical compositional variability of the lithosphere by carrying out a systematic study of peridotitic clinopyroxene and pyrope garnet xenocrysts from four Kaavi–Kuopio kimberlites.

2. Samples

Samples were selected from four kimberlites: the 2-ha Lahtojoki (Pipe no. 7 with 26 cpht of +0.8 mm diamonds), the 2-ha Kylmälahti (no. 17, marginally diamondiferous), the 700 × 30 m Kärenpää (no. 5, diamond grade unknown) and the 300 × 50 m Niilonsuo (no. 2, microdiamond-rich). Xenocryst grains (0.25–2.0 mm) were liberated by lightly crushing the kimberlite material—except for the hard magmatic Niilonsuo kimberlite which was fragmented electrodynamically at Forschungszentrum Karlsruhe—followed by heavy medium separation and hand picking. Hundreds of garnet and clinopyroxene (cpx) xenocrysts as well as 20 garnet-cpx aggregates were recovered from the concentrates. Other mineral phases appropriate for $P–T$ calculations (i.e., orthopyroxene) were not found to coexist with garnet or cpx. Garnets in this study are unsorted and represent the entire range of garnet populations within the kimberlites. However, for the cpx grains, an attempt was made to choose only peridotitic varieties, based on their bright green color.

3. Analytical techniques

Mineral compositions were determined by a Cameca Camebax SX50 electron microprobe (EMP) at the Geological Survey of Finland. For garnet analyses, an acceleration voltage of 25 kV, probe current of 48 nA and beam diameter of 1 μm were applied. The parameters for cpx analyses were 15 kV, 30 nA and 5 μm, respectively. Selected garnet xenocrysts were analyzed for trace elements by LA-ICP-MS at the University of Cape Town using the methodology and equipment described in Grégoire et al. (2003). Detection limits are in the range of 10–20 ppb for Zr and Y and 2 ppm for Ti and Ni. Trace Ni, Mn and Ti data by EMP were obtained on pyrope grains employing 500-nA probe current, 600-s counting times on peak plus background positions and were reduced by the CSIRO TRACE program for the SX50 (Robinson and Graham, 1992). Cross-checking of the two trace methods shows that Ni, Ti and Mn analyses in pyrope by EMP can achieve similar precision to those of LA-ICP-MS down to the level of ca. 10 ppm.

The garnets were classified into harzburgitic, lherzolitic and nonperidotitic varieties according to Gurney (1984); the compositional field for wehrlitic garnet was separated from the lherzolite field using the division of Sobolev et al. (1973). Equilibration pressures and temperatures of the peridotitic cpx xenocrysts were calculated using the single-grain cpx thermobarometer of Nimis and Taylor (2000, NT hereafter). The cpx xenocrysts were screened according to the compositional and crystal structural criteria of Nimis and Taylor (2000) in order to calculate pressures and temperatures only for those grains that had probably coexisted with orthopyroxene and garnet. Xenolith $P–T$ data were calculated using NT and the method of Brey et al. (1990, BKN hereafter). For garnet xenocrysts, the Ni thermometer (Griffin et al., 1989a) was applied using both the calibration of Ryan et al. (1996) and that of Canil (1999).

4. Results

4.1. Garnet major element geochemistry

Representative EMP analyses of garnet xenocrysts are presented in Table 1 and representative garnet analyses from the xenoliths were taken from Peltonen et al. (1999). CaO and Cr_2O_3 contents of pyropes from peridotite xenoliths and pyrope xenocrysts (Fig. 2) show that lherzolitic garnets (G9 according to Dawson and Stephens, 1975) predominate. In addition, orange Ti-rich pyropes of megacryst composition (G1/G2) are common among the xenocrysts. Subcalcic harzburgitic garnets (G10) represent about 6% of the analyzed grains. All of the G10 garnet analyses came from xenocrysts, suggesting that their host

Table 1
Electron microprobe and LA-ICP-MS analyses of garnet xenocrysts from Finnish kimberlites

Sample ID	4682.02	10657.02	4398.96	4403.96	#43	15947.01	15946.01	18279.01	15995.01	#106
Classification	CCGE	CCGE	CCGE	HRZ	HRZ	HRZ	HRZ	HRZ	WHR	WHR
SiO_2 (wt.%)	39.61	40.17	40.83	42.19	41.00	41.05	41.34	41.53	41.03	40.04
TiO_2 (wt.%)	0.05	0.00	0.00	0.03	0.28	0.11	0.31	0.01	0.58	0.53
Al_2O_3 (wt.%)	20.21	17.68	17.00	19.35	17.24	16.81	18.08	16.04	19.20	17.31
Cr_2O_3 (wt.%)	5.01	7.55	8.62	6.05	8.08	8.49	6.59	10.24	4.49	6.89
FeO (wt.%)	8.74	8.25	7.74	6.44	6.22	6.31	6.49	6.27	9.93	8.98
MnO (wt.%)	0.48	0.53	0.56	0.36	0.32	0.32	0.29	0.37	0.50	0.53
MgO (wt.%)	18.35	17.16	17.60	23.19	20.81	21.26	21.04	22.92	17.29	17.58
NiO (wt.%)	0.00	0.00	0.00	0.01	0.01	0.01	0.01	0.01	0.01	0.01
CaO (wt.%)	6.38	7.44	7.67	3.06	5.18	4.24	4.83	2.62	7.28	6.85
Na_2O (wt.%)	0.00	0.00	n.a.	n.a.	n.a.	n.a.	n.a.	n.a.	n.a.	n.a.
K_2O (wt.%)	0.00	0.00	n.a.	n.a.	0.00	0.00	0.00	0.00	0.00	0.00
Total	98.92	98.83	100.08	100.69	99.16	98.68	99.00	100.08	100.33	98.76
Mg/(Mg + Fe)	0.789	0.787	0.802	0.865	0.856	0.857	0.853	0.867	0.756	0.777
Ni (ppm)	12	20	23	50	62	65	65	66	44	46
Y (ppm)	2.8	0.2	0.5	1.1	3	3	3	1.3	25	23
Zr (ppm)	3.8	0.8	2.4	3.9	16	5.7	21	1.2	64	64
T_{Ni} (°C) RGP	687	795	826	1034	1105	1122	1124	1129	993	1006
T_{Ni} (°C) Canil	833	916	938	1082	1127	1137	1139	1142	1055	1064

Sample ID	#94	15,924.01	#9	4674.02	#11	10,635.02	13,358.95	4694.02	18,078.01	4611.02
Classification	WHR	WHR	LHZ	LHZ	LHZ	LHZ	LHZ	LHZ	LHZ	LHZ
SiO_2 (wt.%)	39.99	40.14	40.18	39.58	40.36	40.68	41.13	40.19	41.16	40.37
TiO_2 (wt.%)	0.91	0.88	0.04	0.15	0.61	0.54	0.55	0.35	0.34	0.86
Al_2O_3 (wt.%)	15.99	17.62	17.83	20.11	16.74	19.37	19.75	20.05	17.46	18.67
Cr_2O_3 (wt.%)	7.71	5.70	7.39	4.55	7.86	4.08	4.35	4.88	7.57	5.49
FeO (wt.%)	9.27	9.35	7.85	8.56	8.19	8.52	7.05	6.57	7.03	7.29
MnO (wt.%)	0.42	0.42	0.54	0.42	0.48	0.40	0.41	0.32	0.41	0.38
MgO (wt.%)	17.64	17.84	19.07	19.91	19.04	19.39	20.80	21.72	20.26	20.46
NiO (wt.%)	0.01	0.01	0.00	0.01	0.00	0.01	0.01	0.01	0.01	0.00
CaO (wt.%)	6.87	6.37	5.54	5.20	5.97	5.55	4.83	4.70	5.56	5.32
Na_2O (wt.%)	n.a.	n.a.	n.a.	0.05	n.a.	0.09	n.a.	0.04	n.a.	0.11
K_2O (wt.%)	0.00	0.00	0.00	0.00	0.00	0.00	n.a.	0.00	0.00	0.00
Total	98.82	98.38	98.44	98.59	99.27	98.69	99.06	98.93	99.82	98.99
Mg/(Mg + Fe)	0.772	0.773	0.812	0.806	0.806	0.802	0.840	0.855	0.837	0.833
Ni (ppm)	56	59	21	34	40	46	51	53	55	63
Y (ppm)	17	17	17	13	14	16	11	1.4	1.7	14
Zr (ppm)	50	46	45	46	43	42	28	39	38	45
T_{Ni} (°C) RGP	1071	1084	803	918	964	1004	1040	1050	1061	1109
T_{Ni} (°C) Canil	1106	1114	922	1004	1035	1063	1086	1092	1099	1129

Sample ID	18,065.01	8101.96	10,634.02	18,155.01	18,147.01	18,077.01	4672.02	8114.96	4655.02	18,193.01
Classification	LHZ	LHZ	LHZ	LHZ	LHZ	LHZ	TiP	TiP	TiP	TiP
SiO_2 (wt.%)	40.86	40.65	40.33	41.55	41.44	41.43	40.23	41.30	40.50	41.29
TiO_2 (wt.%)	0.29	0.24	0.89	0.56	0.54	0.56	0.77	0.64	0.64	0.43
Al_2O_3 (wt.%)	16.97	14.50	17.28	18.95	19.45	17.25	20.23	20.74	21.04	22.39
Cr_2O_3 (wt.%)	8.52	10.87	6.28	5.05	4.10	6.96	2.91	1.48	2.16	0.34
FeO (wt.%)	6.55	6.62	8.45	7.06	7.58	6.73	8.50	9.07	8.03	8.89
MnO (wt.%)	0.34	0.39	0.44	0.30	0.28	0.28	0.34	0.37	0.28	0.29
MgO (wt.%)	20.21	19.34	19.02	21.00	21.20	20.91	20.67	20.76	21.31	20.01
NiO (wt.%)	0.00	0.01	0.01	0.01	0.01	0.01	0.01	0.02	0.01	0.01
CaO (wt.%)	5.72	6.70	6.04	5.25	4.80	5.57	5.00	4.23	4.76	5.43

Table 1 (*continued*)

Sample ID	18,065.01	8101.96	10,634.02	18,155.01	18,147.01	18,077.01	4672.02	8114.96	4655.02	18,193.01
Classification	LHZ	LHZ	LHZ	LHZ	LHZ	LHZ	TiP	TiP	TiP	TiP
Na_2O (wt.%)	n.a.	n.a.	0.08	n.a.	n.a.	n.a.	0.06	n.a.	0.04	n.a.
K_2O (wt.%)	0.00	n.a.	0.00	0.00	0.00	0.00	0.00	n.a.	0.00	0.01
Total	99.49	99.48	98.86	99.76	99.42	99.75	98.79	98.79	98.88	99.18
Mg/(Mg + Fe)	0.846	0.839	0.800	0.841	0.833	0.847	0.812	0.803	0.825	0.800
Ni (ppm)	64	71	71	79	84	118	63	71	80	92
Y (ppm)	1.1	20	15	13	14	10	15	16	14	11
Zr (ppm)	25	41	44	43	35	41	43	39	37	23
T_{Ni} (°C) RGP	1117	1154	1155	1196	1222	1383	1108	1155	1201	1264
T_{Ni} (°C) Canil	1135	1157	1158	1182	1198	1288	1129	1157	1186	1222

RGP = Ryan et al. (1996), Canil = Canil (1999); n.a. = not analyzed.

peridotites were more susceptible to fragmentation than other xenolith varieties. Moreover, a well-developed pyrope trend exists in the wehrlitic field similar to that described by Kopylova et al. (1999, 2000) and Carbno and Canil (2002) from the Slave Craton. The trend, named CCGE by Kopylova et al. (2000) after "chromite–clinopyroxene–garnet equilibrium," is characterized by Ca and Cr saturation but shows less enrichment in Cr than the usual lherzolitic trend, and this is taken to indicate that the garnets equilibrated with coexisting cpx and chromite. The Kaavi–Kuopio xenolith record supports this conclusion since the

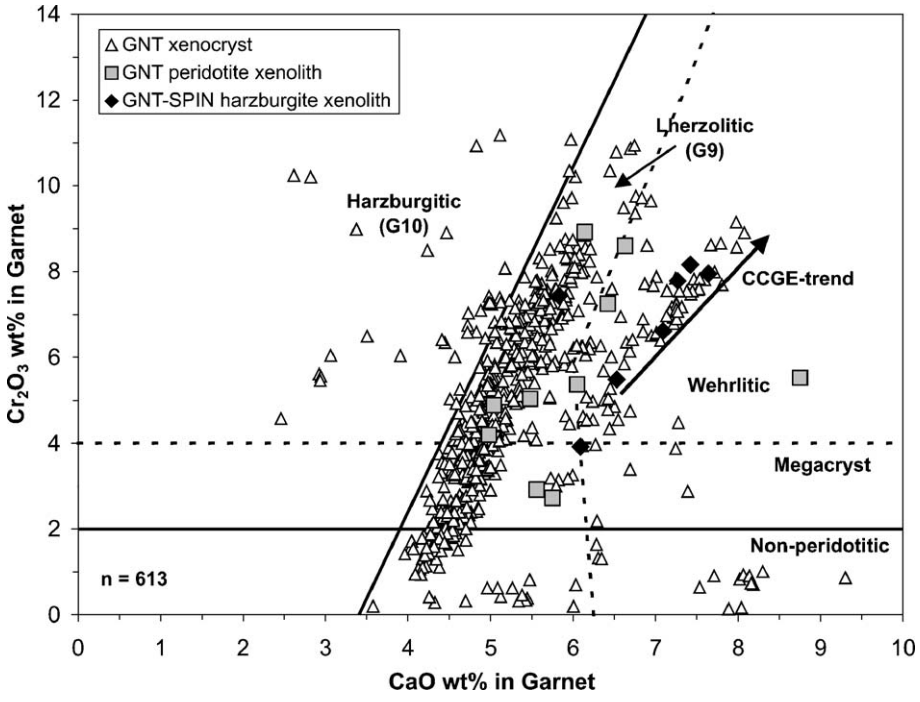

Fig. 2. Cr_2O_3 vs. CaO of Kaavi–Kuopio kimberlite-derived garnets. The xenocryst data are representative of the entire garnet population of the pipes, whereas the xenolith data represent more limited sampling. The harzburgite, lherzolite and nonperidotite fields are redrawn after Gurney (1984) and the wehrlite field is separated according to Sobolev et al. (1973). Arrow marks the "CCGE" garnet trend, i.e., chromite–clinopyroxene–garnet equilibrium, recognized in spinel-garnet peridotites from the Jericho kimberlite (Kopylova et al., 2000).

fine-grained garnet-spinel harzburgite xenoliths with minor amounts (<5%) of secondary cpx (Peltonen et al., 1999) contain garnets that plot along the same CCGE trend.

4.2. Clinopyroxene major element geochemistry

Clinopyroxenes in the garnet-cpx aggregates are chrome diopsides that contain 0.50–4.67 wt.% Cr_2O_3 and 1.21–4.43 wt.% Na_2O. Their Mg/(Mg+Fe) ratios range from 0.90 to 0.94. The corresponding values for the entire cpx xenocryst population that qualified for P–T calculations are 0.50–3.21 wt.% Cr_2O_3, 0.77–3.03 wt.% Na_2O and 0.88–0.96 Mg/(Mg+Fe). Representative EMP analyses of cpx xenocrysts are presented in Table 2. Fig. 3, where cpx analyses from the xenoliths (Peltonen et al., 1999) and xenocrysts (this study) are plotted in a Cr_2O_3 vs. Mg/(Mg+Fe) diagram, shows that the two populations coincide rather well.

The CCGE trend seen in garnet is reflected by cpx geochemistry as described by Kopylova et al. (1999). The cpx grains from garnet-spinel peridotite xenoliths and most of the low-T (<900 °C, NT) cpx xenocrysts show an unusual negative correlation in Mg number and Cr (Fig. 3) due to partitioning of Cr and Mg into

Table 2
Electron microprobe analyses of clinopyroxene xenocrysts from Finnish kimberlites

Sample ID	13,751.01	17,915.01	17,887.01	13,743.01	17,895.01[a]	17,857.01	17,896.01	17,905.01	13,801.01	13,773.01
SiO_2 (wt.%)	54.80	54.61	54.70	55.32	54.98	54.80	54.92	55.34	55.14	54.98
TiO_2 (wt.%)	0.00	0.00	0.29	0.30	0.26	0.22	0.32	0.14	0.33	0.31
Al_2O_3 (wt.%)	1.64	1.34	1.78	2.10	1.54	1.67	1.80	2.50	1.75	1.78
Cr_2O_3 (wt.%)	1.10	0.94	0.87	1.11	1.37	1.39	2.01	1.85	1.92	1.65
FeO (wt.%)	1.36	1.63	2.70	3.22	2.17	2.66	2.30	2.39	2.95	2.55
MnO (wt.%)	0.00	0.01	0.14	0.01	0.11	0.07	0.14	0.00	0.00	0.02
MgO (wt.%)	16.89	17.38	16.29	15.97	16.89	16.48	16.41	16.44	16.93	17.15
NiO (wt.%)	0.08	0.00	0.07	0.03	0.02	0.04	0.09	0.03	0.03	0.02
CaO (wt.%)	22.43	22.55	21.39	20.71	21.11	20.63	20.10	18.96	19.44	19.36
Na_2O (wt.%)	1.12	0.87	1.37	1.82	1.45	1.46	1.75	2.23	1.79	1.75
K_2O (wt.%)	0.04	0.02	0.03	0.01	0.01	0.02	0.01	0.05	0.01	0.03
Total	99.46	99.35	99.63	100.63	99.95	99.44	99.87	99.93	100.28	99.62
Mg/(Mg+Fe)	0.957	0.950	0.915	0.898	0.933	0.917	0.927	0.925	0.911	0.923
T (°C) NT	779	855	881	893	937	975	984	1017	1066	1078
P (kbar) NT	34	37	40	43	45	45	44	45	49	51

Sample ID	13,707.01	#3_104[a]	13,706.01	17,835.01	17,850.01	17,832.01	13,767.01	13,850.01[a]	17,848.01	13,824.01
SiO_2 (wt.%)	55.24	54.43	55.34	55.04	55.22	55.10	55.47	55.45	55.77	55.25
TiO_2 (wt.%)	0.37	0.30	0.37	0.31	0.24	0.29	0.14	0.20	0.23	0.16
Al_2O_3 (wt.%)	1.89	1.71	1.85	1.62	1.48	1.58	1.72	1.73	1.63	2.73
Cr_2O_3 (wt.%)	1.58	1.34	1.41	2.07	2.25	1.76	1.09	0.94	2.62	0.67
FeO (wt.%)	3.00	3.02	3.15	2.27	2.20	2.33	3.30	3.46	3.37	4.53
MnO (wt.%)	0.03	0.03	0.01	0.04	0.08	0.10	0.06	0.05	0.22	0.10
MgO (wt.%)	16.86	17.00	17.30	17.51	17.53	18.19	18.93	19.15	19.07	19.71
NiO (wt.%)	0.05	0.07	0.05	0.02	0.11	0.11	0.06	0.06	0.07	0.07
CaO (wt.%)	18.92	19.13	19.02	18.61	18.52	18.54	17.77	17.49	15.86	14.04
Na_2O (wt.%)	1.97	1.64	1.81	1.83	1.82	1.62	1.33	1.42	1.98	1.89
K_2O (wt.%)	0.03	0.01	0.03	0.04	0.04	0.01	0.03	0.02	0.02	0.01
Total	99.94	98.70	100.44	99.41	99.48	99.63	99.90	100.07	100.89	99.15
Mg/(Mg+Fe)	0.909	0.909	0.907	0.932	0.934	0.933	0.911	0.908	0.910	0.886
T (°C) NT	1091	1102	1117	1140	1157	1190	1279	1292	1309	1364
P (kbar) NT	57	54	56	54	55	54	56	61	57	58

NT = Nimis and Taylor (2000).
[a] Intergrown with garnet.

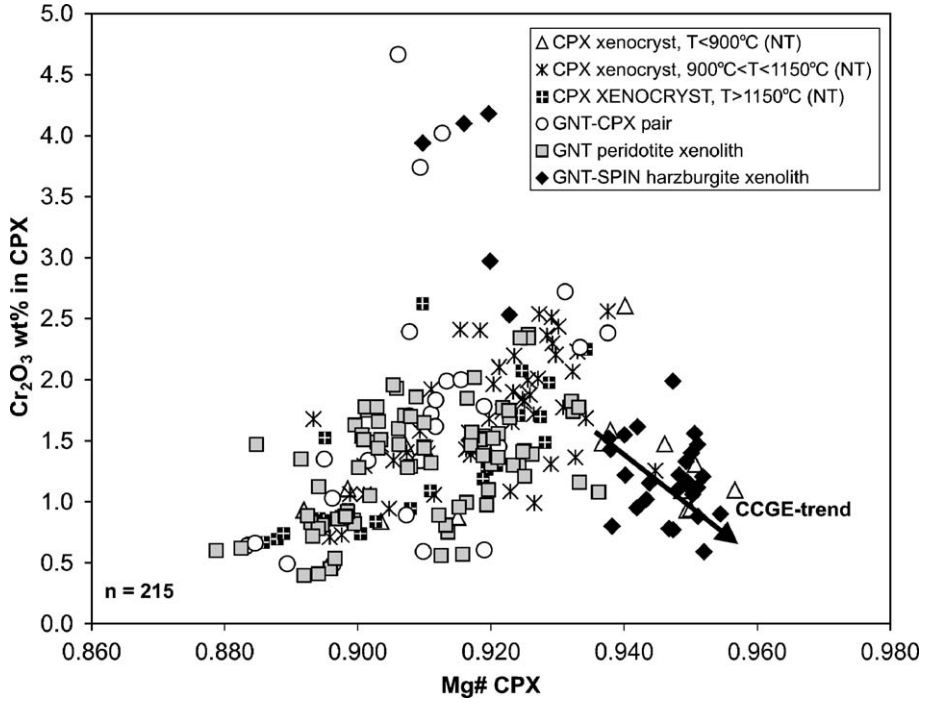

Fig. 3. Cr_2O_3 vs. Mg number for Kaavi–Kuopio clinopyroxenes. The temperatures for cpx xenocrysts are calculated after Nimis and Taylor (2000, NT). Cpx grains from garnet-spinel harzburgites and the low-temperature cpx xenocrysts ($T<900$ °C), in particular, follow the CCGE trend described by Kopylova et al. (1999).

silicate phases controlled by the presence of spinel with a constant Cr/Mg ratio.

4.3. Clinopyroxene thermobarometry

Single-grain cpx thermobarometry fits reasonably well with a geotherm of 36 mW/m^2 calculated using heat flow constraints and Kaavi–Kuopio xenolith modes and geophysical properties (Kukkonen and Peltonen, 1999). Fig. 4 shows the correspondence between the xenolith and xenocryst data. Although there is a shift to lower pressures and slightly lower temperatures in NT results relative to BKN for data from the same xenoliths, these shifts are along the modeled heat flow curves and therefore do not affect the fit of the data to the preferred Kukkonen–Peltonen geotherm (Fig. 4, KP). The BKN P–T values for xenoliths on this geotherm indicate a wide sampling range, approximately 90–230 km. The cpx xenocrysts with compositions along the CCGE trend (Fig. 3) have NT temperatures and pressures in the range of 800–900 °C and 37–41 kbar, respectively, indicating derivation from the same depth range as the garnet-spinel peridotites, i.e., shallower than 130 km according to the local geotherm.

4.4. Garnet thermometry and trace element geochemistry

A subset of the pyrope xenocrysts shown in Fig. 2 was analyzed for trace elements. Representative analyses are presented in Table 1. The T_{Ni} histograms (Fig. 5) show bimodal distributions using both the calibration of Ryan et al. (1996, used hereafter in T_{Ni} values) and that of Canil (1999). The two peaks in the sampling include a strong low-temperature peak at 700–850 °C consisting dominantly of the CCGE pyropes described previously, and a stronger sampling peak at 1000–1150 °C, which includes all but one of the G10 pyropes analyzed for Ni and a second population of more

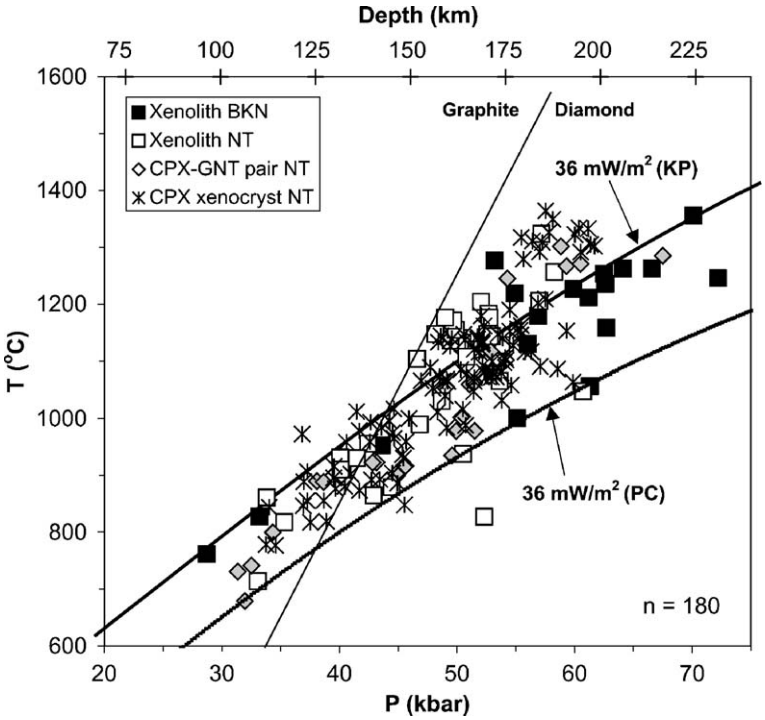

Fig. 4. $P-T$ calculated for xenoliths, cpx-garnet pairs and cpx xenocrysts using the thermobarometers of Brey et al. (1990, BKN) and Nimis and Taylor (2000, NT). Reference model geotherm for 36 mW/m^2 (PC) from Pollack and Chapman (1977) and 36 mW/m^2 (KP) from Kukkonen and Peltonen (1999), the latter calculated for the Karelian craton at 600 Ma. Depth in kilometers is converted from pressure according to Kukkonen et al. (2003). The diamond–graphite transition is redrawn after Kennedy and Kennedy (1976).

typical wehrlitic grains (i.e., with compositions that do not plot along the CCGE trend). In addition to being the highest temperature at which the latter two pyrope types occur, 1150 °C also represents a break in the stratigraphic section of the lithosphere based on the Zr and Y contents of garnets, separating mantle that contains strongly depleted pyropes from more enriched mantle (Fig. 6). The intermediate temperature (1000–1150 °C) wehrlitic population is enriched in Y and Zr relative to all other pyrope varieties (Fig. 6) and to the ultra-depleted low-temperature CCGE garnets in particular. Fig. 6 also shows megacryst composition Ti-rich pyropes (TiPs), which have an enigmatic origin, but are nevertheless included here for illustrative purposes. We defend the reasoning for plotting at least the most Mg-rich TiPs on these diagrams as they reach the same Mg and Cr contents as lherzolitic pyropes, implying equilibration with olivine similar to that in the lherzolites. The great majority of these Mg-rich TiP analyses plot at temperatures above the 1150 °C edge.

The two breaks in the mantle stratigraphy underlying Kaavi–Kuopio also show up well using TiO_2 contents of the pyropes, as seen in Fig. 7, where the T_{Ni} temperatures have been extrapolated to the local geotherm (Kukkonen and Peltonen, 1999) to give pressures and depths for each grain. Overall, the garnet xenocrysts cover a sampling interval from 80 to 230 km, without any major discontinuities. The main horizon of sampling at 1000–1150 °C corresponds to the mantle section from 140 to 180 km, from which only few xenoliths have been recovered. The lower temperature boundary at about 850 °C corresponds to the break in TiO_2 at approximately 110 km depth above which only extremely low TiO_2 content pyropes exist, most of these being CCGE in composition. The second boundary roughly at 1150

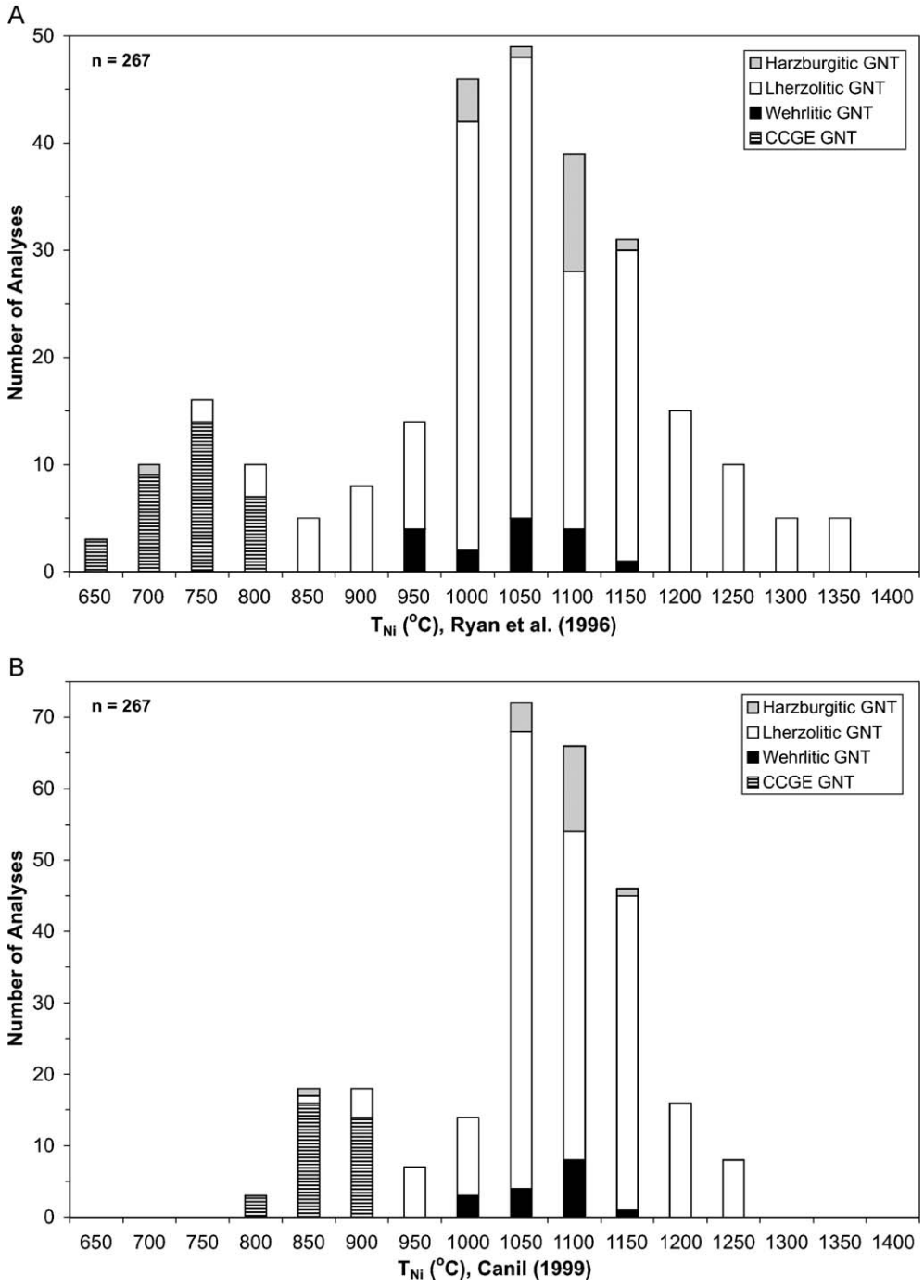

Fig. 5. Distribution of T_{Ni} for trace element analyzed Kaavi–Kuopio pyrope xenocrysts comparing the calibrations of (A) Ryan et al. (1996) and (B) Canil (1999).

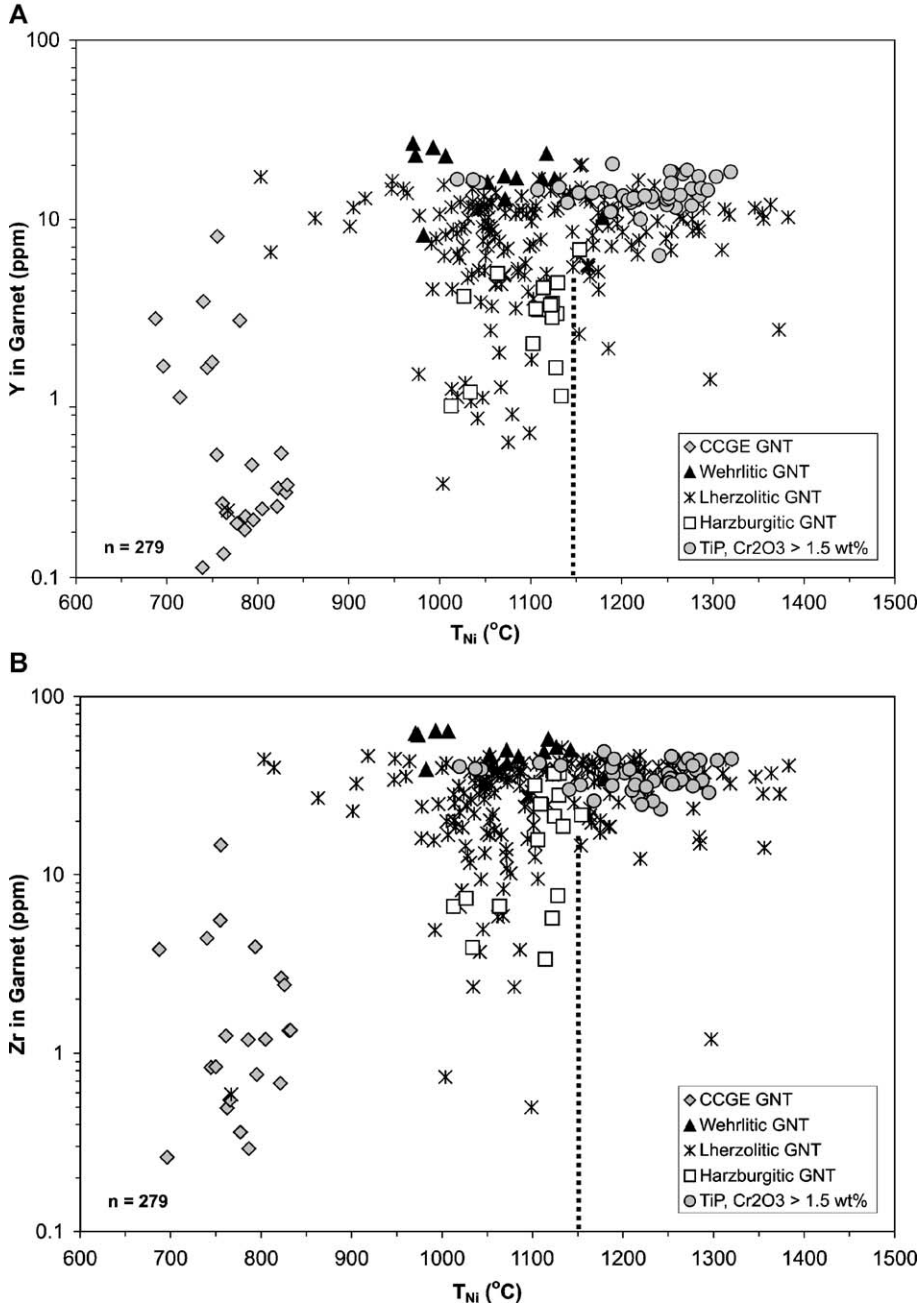

Fig. 6. (A) Y and (B) Zr contents of pyropes vs. T_{Ni} (Ryan et al., 1996) both show an edge at about 1150 °C. The edge does not mark the lower boundary of the lithosphere, as all xenoliths from >1150 °C are coarse granular peridotites typical of subcontinental lithospheric mantle.

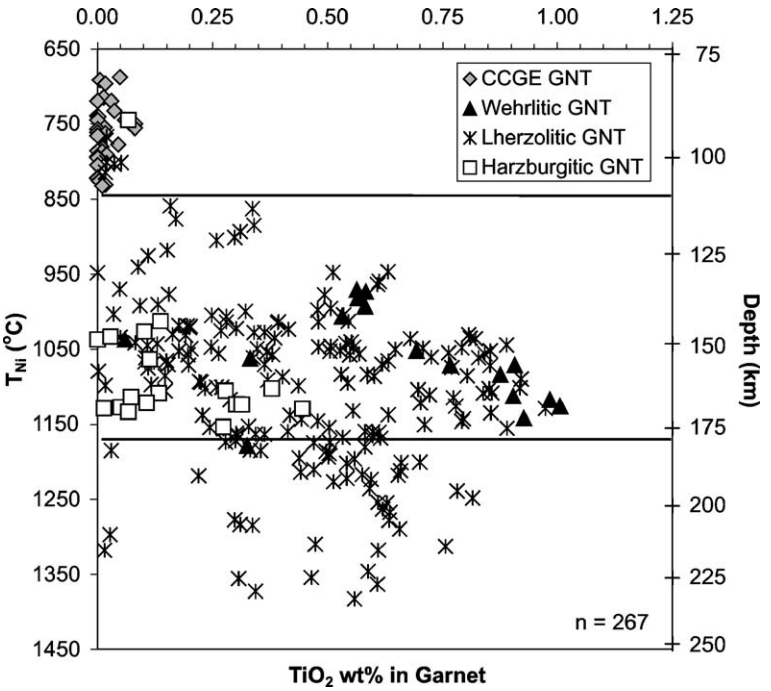

Fig. 7. TiO_2 vs. T_{Ni} (Ryan et al., 1996) and depth for the Kaavi–Kuopio pyropes showing three distinct layers of the underlying mantle. Depths are calculated by extrapolating the T_{Ni} temperatures of pyropes to the local geotherm of Kukkonen and Peltonen (1999).

°C or ca. 180 km is the limit below which only a very few TiO_2-depleted pyropes occur.

5. Discussion

5.1. The CCGE trend in garnet

The compositional trend of Ca- and Cr-saturated garnets (CCGE) seen in the Kaavi–Kuopio garnet-spinel peridotites and low-T garnet xenocrysts is only rarely observed in kimberlites or associated xenoliths. Kopylova et al. (1999, 2000) and Carbno and Canil (2002) described it from garnet-spinel peridotite xenoliths in the Jericho and Drybones Bay kimberlites in the Slave Craton. Similar garnets are also found in minor proportion in the Ranch Lake kimberlite concentrate (Cookenboo, 1996). The few other localities with this type of trend include the chromite-bearing garnet lherzolites from the Thumb primitive minette in the Colorado Plateau (Ehrenberg, 1982; Smith et al., 1991), which show the trend strongly, and a set of rare peridotites from the Lesotho xenolith suite (Smith and Boyd, 1992).

Smith and Boyd (1992) noted that the CCGE trend parallels the compositional trend in garnet produced by experiments on natural (spinel-bearing) lherzolite (Brey et al., 1990). The CCGE garnets from Kaavi–Kuopio are plotted in Fig. 8, along with the compositional fields for garnets from Jericho (Kopylova et al., 1999, 2000), Thaba Putsoa, Lesotho (Smith and Boyd, 1992) and the lherzolite experiments (Brey et al., 1990). The Kaavi–Kuopio CCGE trend parallels that of the other two kimberlites, but at lower temperatures and pressures, and cuts slightly across the isotherms derived from the experimental data. The temperatures and pressures estimated from Fig. 8 for Kaavi–Kuopio CCGE-bearing xenoliths are reasonably consistent with the P–T of the cpx from these xenoliths and the T_{Ni} values of the garnets (Fig. 5). Taken together, this indicates derivation from temperatures and pressures below 900 °C and 40 kbar, i.e., shallower than 130 km according to the local geotherm.

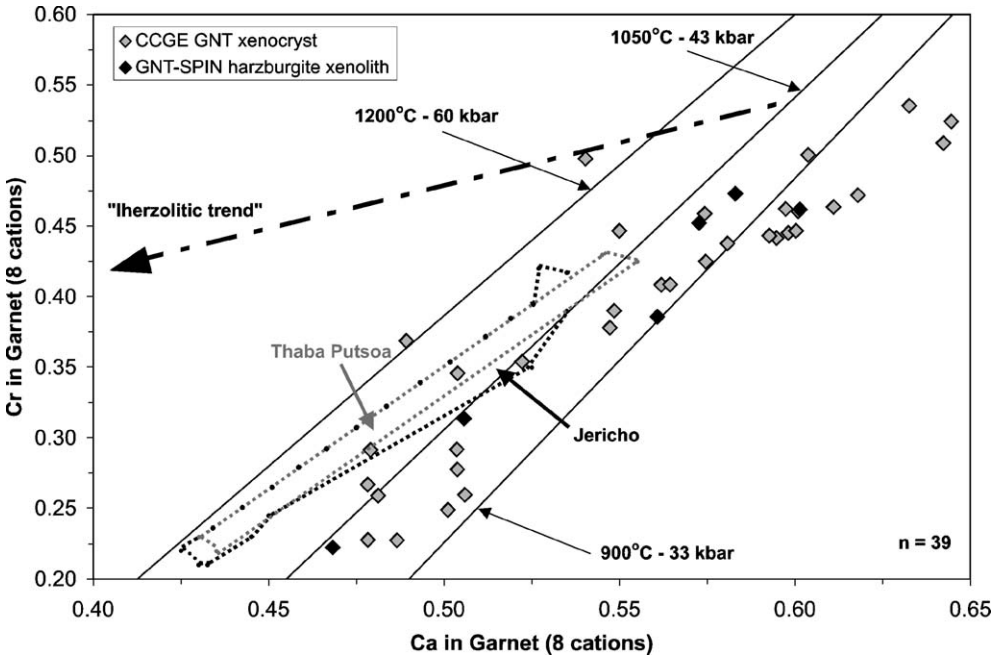

Fig. 8. Ca–Cr diagram for garnet showing the Kaavi–Kuopio CCGE xenocrysts and garnets from garnet-spinel harzburgite xenoliths. For comparison, the spinel-garnet equilibration trends from Jericho (Kopylova et al., 1999), Thaba Putsoa, Lesotho (Smith and Boyd, 1992) and from experiments on natural lherzolite compositions at 900–1200 °C and 33–60 kbar (Brey et al., 1990). Arrow denotes the common lherzolitic trend.

Kopylova et al. (2000) concluded that Ca-saturated cpx-bearing garnet-spinel cratonic peridotites are restricted to mantle segments of special character since Cr-rich rocks are normally poor in Ca and vice versa. Garnet and spinel-bearing mantle, which is harzburgitic under most Archean cratons (Griffin et al., 1999a), tends to be too depleted to provide sufficient cpx for development of the CCGE trend. Moreover, the rarity of the trend may derive from the disequilibrium between phases in cratonic spinel-garnet peridotites (Kopylova et al., 2000; Smith and Boyd, 1992). The mantle beneath Jericho (Kopylova et al., 2000) and the Colorado Plateau (Ehrenberg, 1982) are special because their spinel-garnet mantle is lherzolitic or cpx-bearing harzburgitic. These locations are also characterized by the complete absence of subcalcic harzburgitic garnet (G10) and the presence of lherzolitic Ca-saturated garnet at all mantle depths (Kopylova et al., 2000; Griffin and Ryan, 1995). The Kaavi–Kuopio mantle segment is similar to that of Jericho in the respect that the CCGE trend derives from garnets in garnet-spinel harzburgites with minor amounts (<5%) of cpx. However, despite this similarity in host rock for the CCGE garnets, the Kaavi–Kuopio mantle also differs significantly from that of Jericho (and the Colorado Plateau) since it contains G10s in the deeper layers of the lithosphere, and moreover, one G10 grain falls within the temperature range of the CCGE garnets (Fig. 7). Overall, the CCGE trend in Kaavi–Kuopio exists only in a narrow, upper layer of the lithosphere (<120 km), as its lower parts are of a completely different nature.

The ultradepletion of CCGE garnets with respect to Ti, Y and Zr, combined with their contradictory saturation in Ca, indicate that their host peridotite was not produced by a single partial melting event of the primitive mantle. The CCGE garnets may have been derived from a mantle source that has been ultradepleted by melt extraction and later refertilized in Ca by some chemical enrichment process such as carbonatite metasomatism (Kopylova et al., 2000; Carbno and Canil, 2002). The addition of Ca led to crystallization of secondary cpx (as seen in Kaavi–Kuopio garnet-spinel facies xenoliths) and the trans-

formation of harzburgitic garnets to wehrlitic. The transformation from harzburgite to lherzolite has been described from mantle garnets from suites in Kimberley, South Africa (Schulze, 1995; Griffin et al., 1999b). In contrast to the peridotitic minerals in the mantle beneath Jericho (Kopylova et al., 1999) and the Colorado Plateau (Smith and Ehrenberg, 1984; Smith et al., 1991), the Kaavi–Kuopio grains do not display extensive zoning that would indicate such secondary refertilization. This suggests that there was sufficient time for equilibration with the metasomatizing agents. This conclusion is also supported by the garnet-cpx Sm–Nd isochrons of garnet-spinel facies xenoliths that yield ages of 600 Ma (Peltonen et al., 1999), the same age as the host kimberlites, suggesting continuous re-equilibration of garnets at mantle temperatures up to the time of emplacement.

Based on the whole rock REE abundances, regional geology and model presented for the local geodynamic evolution, Peltonen et al. (1999) concluded that the low-*T* garnet-spinel peridotites could represent harzburgitic residues, i.e., remnants of the reworked Archean lithosphere, metasomatized shortly before or during the invasion of a kimberlite-derived melt or fluid completely obscuring their ancient isotopic signature. Carbno and Canil (2002), however, suggested that the abundance of ultradepleted (Zr, Y, Ti) but Ca-enriched garnets in Drybones Bay kimberlite may be explained by carbonatite metasomatism, where cpx forms from opx as a result of the interaction of carbonate melt with harzburgite (Yaxley et al., 1998).

5.2. The 180-km boundary

The petrographic evidence for modal metasomatism seen in the Kaavi–Kuopio garnet facies xenoliths (Peltonen et al., 1999) is in agreement with the garnet xenocrysts. The Y–Zr diagram (Fig. 9) shows that the xenocryst record is comprised of depleted and melt metasomatized grains. The wehrlitic pyropes, in particular, preserve evidence of melt metasomatism, whereas the lherzolitic grains show this chemical signature to a lesser extent. Most of the harzburgitic

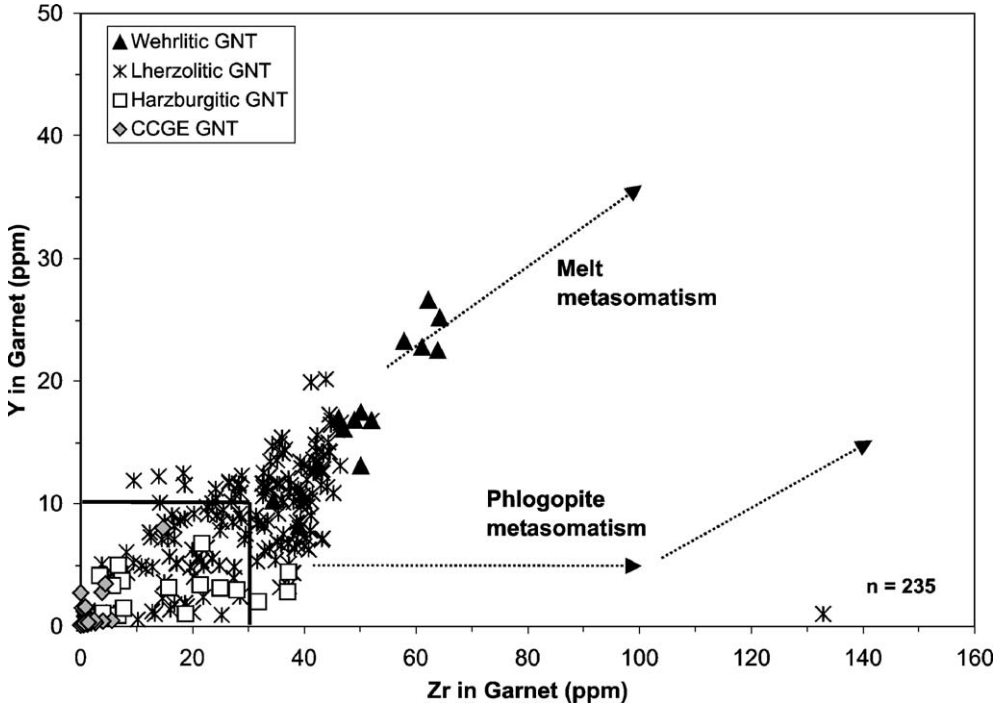

Fig. 9. Plot of Y and Zr for the Kaavi–Kuopio pyrope xenocrysts. Melt and phlogopite metasomatism trends after Griffin et al. (1999b). Solid black line defines the depleted field.

and all of the CCGE xenocrysts plot in the "depleted" field.

As illustrated in Figs. 6 and 7, there is a distinct upper temperature limit for strongly depleted garnets defined by low Ti, Zr and Y contents at 1150 °C (T_{Ni}), corresponding to a depth of 180 km on the local geotherm. According to Griffin and Ryan (1995), this kind of garnet composition "edge" marks the position of the inferred base of the lithosphere. Another interpretation, however, is supported by the existence of a few depleted garnet xenocrysts of T_{Ni}—temperatures higher than 1150 °C in the Kaavi–Kuopio suite (Figs. 6 and 7). These are significant because they may represent remnants of a previously existing depleted layer or deeper extension of the 130–180 km layer that was refertilized by melt metasomatism. Such metasomatism could have caused the destruction of all previously existing harzburgitic material in this layer and forced the crystallization of abundant Ti-rich pyropes.

The T_{Ni} of the compositional edge in garnet also corresponds to the "kink" or "step" seen in xenolith geotherms from various kimberlite fields (Griffin and Ryan, 1995) reflecting a change from an essentially conductive geotherm to a steeper temperature gradient (Finnerty and Boyd, 1987; Griffin and Ryan, 1995). Xenoliths along the "kink" or above the high-T "step" of the geotherm commonly have foliated microstructures and show geochemical evidence of infiltration by asthenosphere-derived melts (Smith et al., 1991; Griffin et al., 1989b). However, none of the Kaavi–Kuopio xenoliths, from a stratigraphic record that goes down to 240 km, shows any of the textural or geochemical features of sheared high-T peridotites (Kukkonen and Peltonen, 1999). Thus, the 1150 °C/180-km edge determined by the garnet compositional break does not mark the base of the lithospheric mantle at Kaavi–Kuopio, but instead represents a sublithospheric mantle compositional discontinuity.

6. Conclusions

Lithosphere mantle xenoliths in Group I kimberlites from the Kaavi–Kuopio area of Eastern Finland provide evidence of a stratified mantle underlying the SW margin of the Archean Karelian Craton. This craton edge has experienced a complicated history including rifting around 1.95 Ga and continental collision around 1.88 Ga (Nironen, 1997; Peltonen et al., 1998), and consequently, the mantle stratigraphy is complex. With the present resolution, at least three lithospheric mantle layers can be distinguished (Fig. 10): (1) an upper layer, shallower than 130 km, composed of secondary cpx-bearing CCGE pyrope-spinel harzburgites; (2) a middle garnet peridotite layer, from 130 to 180 km, ranging from lherzolite to harzburgite to wehrlite; and (3) a lower, more fertile layer, from 180 to 240 km, from where the bulk of the garnet facies peridotite and eclogite xenoliths were derived.

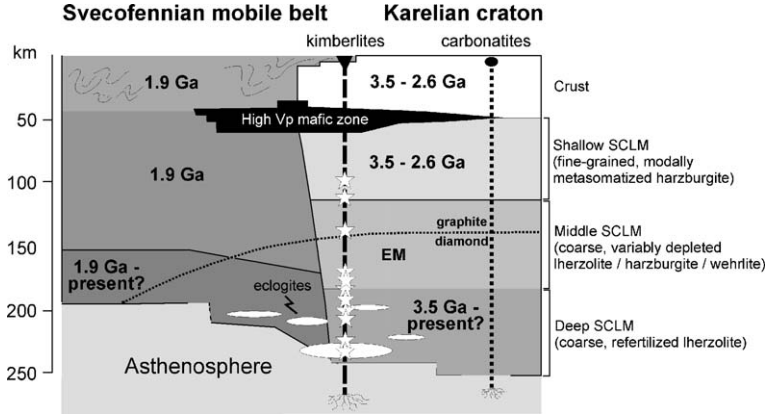

Fig. 10. Schematic cross section through the rifted and redocked edge of the Karelian craton showing the three distinct petrologic layers in the mantle inferred from pyrope and xenolith compositions. Stars mark the depth of origin of the xenoliths based on BKN thermobarometry.

The ages of these distinct mantle layers are still to be resolved, but we believe at least the middle, and likely the upper layer, to be Archean, with a similar age to that of the overlying crust. The lowermost layer may represent Archean mantle that has been considerably refertilized by melt metasomatism. This is supported by the few low-Ti pyropes thought to be from this depth and representing remnant depleted material. Alternatively, it is possible that this section of the mantle has been tectonically emplaced during the collision event at 1.88 Ga. In terms of diamond prospectivity, the graphite–diamond stability curve (Kennedy and Kennedy, 1976) transects the middle mantle layer and implies a diamond window in the Kaavi–Kuopio mantle between 140 and 180 km, defined by the lower temperature stability limit of diamond and the deepest extent to which G10 garnets occur, a roughly 40-km-thick prospective zone. Additionally, a well-sampled component of diamondiferous eclogites adds considerably to the diamond potential of this mantle.

Acknowledgements

This study was funded by the Geological Survey of Finland and the Academy of Finland. Professor John Gurney and Dr. Andreas Späth from the University of Cape Town are acknowledged for the access to the LA-ICP-MS instrument. We are also grateful to the head of the GTK Research Laboratory, Dr. Jukka Marmo, as well as the laboratory personnel for their encouragement and skillful assistance. The support of Professor Ilmari Haapala from the University of Helsinki is appreciated.

References

Brey, G.P., Köhler, T., Nickel, K.G., 1990. Geothermobarometery in four-phase lherzolites: I. Experimental results from 10 to 60 kb. J. Petrol. 31, 1313–1352.

Calcagnile, G., 1982. The lithosphere-asthenosphere system in Fennoscandia. Tectonophysics 90, 19–35.

Canil, D., 1999. The Ni-in-garnet geothermometer: calibration at natural abundances. Contrib. Mineral. Petrol. 136, 240–246.

Carbno, G.B., Canil, D., 2002. Mantle structure beneath the SW Slave Craton, Canada: constraints from Garnet Geochemistry in the Drybones Bay kimberlite. J. Petrol. 43 (1), 129–142.

Cookenboo, H., 1996. Ranch Lake kimberlite in the Central Slave Craton: the mantle sample. The Gangue, vol. 52, Geol. Assoc. of Canada, Miner. Deposits Div., Victoria, Canada, pp. 12–13.

Dawson, J.B., Stephens, W.E., 1975. Statistical analysis of garnets from kimberlites and associated xenoliths. J. Geol. 83, 589–607.

Ehrenberg, S.N., 1982. Petrogenesis of garnet lherzolite and megacrystalline nodules from the Thumb, Navajo volcanic field. J. Petrol. 23 (4), 507–547.

Finnerty, A.A., Boyd, F.R., 1987. Thermobarometry for garnet peridotites: basis for the determination of thermal and compositional structure of the upper mantle. In: Nixon, P.H. (Ed.), Mantle Xenoliths. Wiley, Chichester, pp. 381–412.

Gaál, G., Gorbatschev, R., 1987. An outline of the Precambrian evolution of the Baltic Shield. Precambrian Res. 35, 15–52.

Grégoire, M., Bell, D.R., le Roex, A.P., 2003. Garnet lherzolites from the Kaapvaal craton (South Africa): trace element evidence for a metasomatic history. J. Petrol. 44 (4), 629–657.

Griffin, W.L., Ryan, C.G., 1995. Trace elements in indicator minerals: area selection and target evaluation in diamond exploration. In: Griffin, W.L. (Ed.), Diamond Exploration: Into the 21st Century. J. Geochem. Explor., vol. 53, pp. 311–337.

Griffin, W.L., Cousens, D.R., Ryan, C.G., Sie, S.H., Suter, G.F., 1989a. Ni in chrome pyrope garnets: a new geothermometer. Contrib. Mineral. Petrol. 103, 199–202.

Griffin, W.L., Smith, D., Boyd, F.R., Cousens, D.R., Ryan, C.G., Sie, S.H., Suter, G.F., 1989b. Trace element zoning in garnets from sheared mantle xenoliths. Geochim. Cosmochim. Acta 53, 561–567.

Griffin, W.L., Fisher, N.I., Friedman, J., Ryan, C.G., O'Reilly, S.Y., 1999a. Cr-pyrope garnets in the lithospheric mantle: I. Compositional systematics and relations to tectonic setting. J. Petrol. 40 (5), 679–704.

Griffin, W.L., Shee, S.R., Ryan, C.G., Win, T.T., Wyatt, B.A., 1999b. Harzburgite to lherzolite and back again: metasomatic processes in ultramafic xenoliths from the Wesselton kimberlite, Kimberley, South Africa. Contrib. Mineral. Petrol. 134, 232–250.

Gurney, J.J., 1984. A correlation between garnets and diamonds. In: Glover, J.E., Harris, P.G. (Eds.), Kimberlite Occurrence and Origin: A Basis for Conceptual Models in Exploration, vol. 8, University of Western Australia, Perth, Australia, pp. 143–166.

Kennedy, C.S., Kennedy, G.C., 1976. The equilibrium boundary between graphite and diamond. J. Geophys. Res. 81, 2467–2470.

Kontinen, A., Paavola, J., Lukkarinen, H., 1992. K–Ar ages of hornblende and biotite from Late Archean rocks of eastern Finland; interpretation and discussion of tectonic implications. Geol. Surv. Finland Bull. 365 (31 pp.).

Kopylova, M.G., Russell, J.K., Cookenboo, H., 1999. Petrology of peridotite and pyroxenite xenoliths from the Jericho kimberlite: implications for the thermal state of the mantle beneath the Slave Craton, northern Canada. J. Petrol. 40 (1), 79–104.

Kopylova, M.G., Russell, J.K., Stanley, C., Cookenboo, H., 2000. Garnet from Cr- and Ca-saturated mantle: implications for diamond exploration. J. Geochem. Explor. 68, 183–199.

Kukkonen, I.T., Jõeleht, A., 1996. Geothermal modelling of the lithosphere in the central Baltic Shield and its southern slope. Tectonophysics 255, 24–45.

Kukkonen, I.T., Peltonen, P., 1999. Xenolith controlled geotherm for the central Fennoscandian Shield: implications for lithosphere–asthenosphere relations. Tectonophysics 304 (4), 301–315.

Kukkonen, I.T., Kinnunen, K.A., Peltonen, P., 2003. Mantle xenoliths and thick lithosphere in the Fennoscandian shield. Phys. Chem. Earth 28 (9–11), 349–360.

Nimis, P., Taylor, W.R., 2000. Single clinopyroxene thermobarometry for garnet peridotites: Part I. Calibration and testing of a Cr-in-cpx barometer and an enstatite-in-Cpx thermometer. Contrib. Mineral. Petrol. 139, 541–554.

Nironen, M., 1997. The Svecofennian orogen: a tectonic model. Precambrian Res. 86, 21–44.

O'Brien, H.E., Tyni, M., 1999. Mineralogy and geochemistry of kimberlites and related rocks from Finland. In: Gurney, J.J., Gurney, J.L., Pascoe, M.D., Richardson, S.H. (Eds.), Proceedings of the 7th International Kimberlite Conference. Red Roof Design cc, Cape Town, South Africa, pp. 625–636.

O'Brien, H.E., Peltonen, P, Vartiainen, H., in press. Kimberlites, carbonatites and alkaline rocks. In: Lehtinen, M., Nurmi, P.A., Rämö, O.T. (Eds.), Precambrian Geology of Finland—Key to the Evolution of the Fennoscandian Shield. Elsevier Science, Amsterdam.

Peltonen, P., Mänttäri, I., 2001. An ion microprobe U–Th–Pb study of zircon xenocrysts from the Lahtojoki kimberlite pipe, eastern Finland. Bull. Geol. Soc. Finl. 73, 47–58.

Peltonen, P., Kontinen, A., Huhma, H., 1998. Petrogenesis of the mantle sequence of the Jormua Ophiolite (Finland): melt migration in the upper mantle during Palaeoproterozoic continental break-up. J. Petrol. 39, 297–329.

Peltonen, P., Huhma, H., Tyni, M., Shimizu, N., 1999. Garnet peridotite xenoliths from kimberlites of Finland: nature of the continental mantle at an Archaean craton—Proterozoic mobile belt transition. In: Gurney, J.J., Gurney, J.L., Pascoe, M.D., Richardson, S.H. (Eds.), Proceedings of the 7th International Kimberlite Conference. Red Roof Design cc, Cape Town, South Africa, pp. 664–675.

Peltonen, P., Kinnunen, K.A., Huhma, H., 2002. Petrology of two diamondiferous eclogite xenoliths from the Lahtojoki kimberlite pipe, eastern Finland. Lithos 63 (3–4), 151–164.

Pollack, H.N., Chapman, D.S., 1977. On the regional variations of heat flow, geotherms and lithosphere thickness. Tectonophysics 38, 279.

Robinson, B.W., Graham, J., 1992. Advances in electron microprobe trace element analysis. J. Comput.-Assist. Microsc. 4, 263–265.

Ryan, C.G., Griffin, W.L., Pearson, N.J., 1996. Garnet geotherms: pressure–temperature data from Cr-pyrope garnet xenocrysts in volcanic rocks. J. Geophys. Res. 101, 5611–5625.

Schulze, D.J., 1995. Low-Ca garnet harzburgites from Kimberley, South Africa: abundance and bearing on the structure and evolution of the lithosphere. J. Geophys. Res. 100 (12), 513–526.

Smith, D., Boyd, F.R., 1992. Compositional zonation in garnets in peridotite xenoliths. Contrib. Mineral. Petrol. 112, 134–147.

Smith, D., Ehrenberg, S.N., 1984. Zoned minerals in garnet peridotite nodules from the Colorado plateau: implications from mantle metasomatism and kinetics. Contrib. Mineral. Petrol. 86, 274–285.

Smith, D., Griffin, W.L., Ryan, C.G., Sie, S.H., 1991. Trace-element zonation in garnets from the Thumb: heating and melt infiltration below the Colorado Plateau. Contrib. Mineral. Petrol. 107, 60–79.

Sobolev, N.V., Lavrentiev, Yu.G., Pokhilenko, N.P., Usova, N.P., 1973. Chrome-rich garnets from the kimberlites of Yakutia and their paragenesis. Contrib. Mineral. Petrol. 40, 39–52.

Tyni, M., 1997. Diamond prospecting in Finland—a review. In: Papunen, H. (Ed.), Mineral Deposits: Research and Exploration, Where do They Meet? Proceedings of the 4th SGA Meeting. A.A. Balkema, Rotterdam, pp. 789–791.

Yaxley, G.M., Green, D.H., Kamenetsky, V., 1998. Carbonatite metasomatism in the southeastern Australian lithosphere. J. Petrol. 39, 1917–1930.